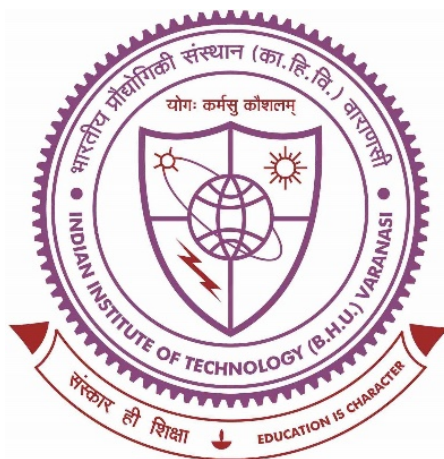


Design, Synthesis, and Biological Evaluation of Quinazoline Derivatives as Multi-targeting Agents in the Treatment of Alzheimer's Disease



Thesis submitted in partial fulfilment for the
Award of Degree

DOCTOR OF PHILOSOPHY

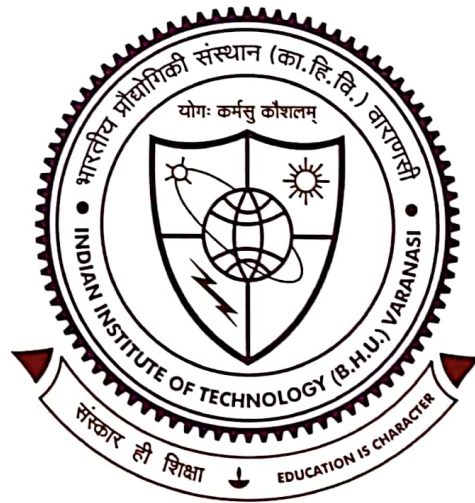
By

Akash Verma

Department of Pharmaceutical Engineering & Technology
Indian Institute of Technology
(Banaras Hindu University)
Varanasi-221005 India

Roll No.19161012

2024





भारतीय
प्रौद्योगिकी
संस्थान
काशी हिन्दू विश्वविद्यालय



INDIAN
INSTITUTE OF
TECHNOLOGY
BANARAS HINDU UNIVERSITY

Department of Pharmaceutical Engineering and Technology

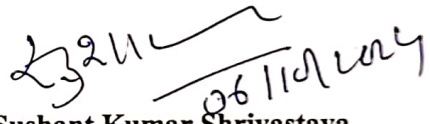
CERTIFICATE

It is certified that the work contained in the thesis titled “**Design, Synthesis, and Biological Evaluation of Quinazoline Derivatives as Multi-targeting Agents in the Treatment of Alzheimer’s Disease**” by **Mr. Akash Verma** has been carried out under my supervision and that this work has not been submitted elsewhere for a degree.

It is further certified that the student has fulfilled all the requirements of Comprehensive Examination, Candidacy, and SOTA for the award of Ph.D. Degree.

Date: 06/10/2024

Place: IIT (BHU), Varanasi


Prof. Sushant Kumar Shrivastava
(Supervisor)

Dr. S. K. SHRIVASTAVA
Professor
Deptt. of Pharm. Engg. and Tech
Indian Institute of Technology
(Banaras Hindu University)
Varanasi-221005



भारतीय
प्रौद्योगिकी
संस्थान
काशी हिन्दू विश्वविद्यालय



INDIAN
INSTITUTE OF
TECHNOLOGY
BANARAS HINDU UNIVERSITY

Department of Pharmaceutical Engineering and Technology

DECLARATION BY THE CANDIDATE

I, **Akash Verma**, certify that the work embodied in this Ph.D. thesis is my own bonafide work, and was carried out by me under the supervision of **Prof. Sushant Kumar Shrivastava** from July 2019 to July 2024 at the **Department of Pharmaceutical Engineering & Technology, Indian Institute of Technology (Banaras Hindu University), Varanasi**. The matter embodied in this Ph.D. thesis has not been submitted for the award of any other degree/diploma.

I declare that I have faithfully acknowledged and given credit to the research workers wherever their works have been cited in my work in this thesis. I further declare that I have not willfully copied any other's work, paragraphs, text, data, results, etc. reported in the journals, books, magazines, reports, dissertations, theses, etc., or available at websites and have not included them in this Ph.D. thesis and have not cited as my own work.

Date: 06/10/2024

Place: IIT (BHU), Varanasi

Akash Verma

Akash Verma

It is certified that the above statement made by the student is correct to the best of our knowledge.

CERTIFICATE BY THE SUPERVISOR AND HEAD OF THE DEPARTMENT

Sushant Kumar Shrivastava
Prof. Sushant Kumar Shrivastava
(Supervisor)

Dr. S. K. SHRIVASTAVA
Professor
Deptt. of Pharm. Engg. and Tech
Indian Institute of Technology
(Banaras Hindu University)
Varanasi-221005

S. Hemalatha 7/10/24
(Head of the Department)
विभागाध्यक्ष / Head

भैषजकीय अभियांत्रिकी एवं प्रौद्योगिकी विभाग /
Department of Pharmaceutical Engineering & Technology
भारतीय प्रौद्योगिकी संस्थान / INDIAN INSTITUTE OF TECHNOLOGY
(बनारस हिन्दू विश्वविद्यालय) / (BANARAS HINDU UNIVERSITY)
वाराणसी-२२१००५ / Varanasi-221005 iii



भारतीय
प्रौद्योगिकी
संस्थान
काशी हिन्दू विश्वविद्यालय



INDIAN
INSTITUTE OF
TECHNOLOGY
BANARAS HINDU UNIVERSITY

Department of Pharmaceutical Engineering and Technology

COPYRIGHT TRANSFER CERTIFICATE

Title of the Thesis : Design, Synthesis, and Biological Evaluation of Quinazoline
Derivatives as Multi-targeting Agents in the Treatment of
Alzheimer's Disease

Candidate's Name : Mr. Akash Verma

Copyright Transfer

The undersigned hereby assigns to the Indian Institute of Technology (Banaras Hindu University), Varanasi all rights under copyright that may exist in and for the above thesis submitted for the award of the Ph.D. degree.

Date: 06/10/2024

Akash Verma

Place: IIT (BHU), Varanasi

Akash Verma

Note: However, the author may reproduce or authorize others to reproduce material extracted verbatim from the thesis or derivative of the thesis for the author's personal use provided that the source and University's copyright notice are indicated.

Acknowledgments

I bow to the feet of ***Bharat Ratna Pandit Madan Mohan Malaviyaji***, founder of the Banaras Hindu University which is his crowning achievement. Living in his abode, I always felt a sense of holiness. It is a stupendous monument to his peculiar genius, his audacity in conception, and his persistence in execution. The University symbolizes Malviyaji's respect for the past, confidence in the present, and hope for the future generation of India.

It is a matter of privilege and joy to express my feelings of gratitude to ***Prof. Sushant Kumar Shrivastava***. I am thankful for his continuous support throughout my research for his patience, motivation, and immense knowledge. I am indebted to him for his appreciation for success and backing and support in failures, which ultimately made me keen to tackle any obstructions occurring during the research work. Without his supervision and constant help, this dissertation would not have been possible. He also helped me a lot as Head, of the Department of Pharmaceutical Engineering & Technology, Indian Institute of Technology (Banaras Hindu University), Varanasi to use the department facilities to carry out my research work.

I am also grateful to, ***Prof. B. Mishra, Prof. S.K. Singh & Prof. Sanjay Singh***, Former Heads, for their constant inspiration, valuable suggestions, and help which have led to the successful completion of this work.

I owe my gratitude to all my respected Research Progress and Evaluation Committee (RPEC) members for their encouragement and insightful comments leading me to the completion of the research work.

I would like to thank ***Prof. Sairam Krishnamurthy*** for their continuous support in performing *in vivo/ex vivo* experiments.

My sincere thanks also goes to ***Dr. Mutthu, Dr. Senthil Raja, Dr. Gyan Prakash Modi, Dr. A. N. Sahu, Dr. Vinod Tiwari, Dr. Ruchi Chawla, Dr. A.K. Mourya, Dr. S.K. Mishra, Dr. Shreyans, Dr. Ashish, Dr. Rajnish, Dr. Deepak, and Dr. Jairam*** for their constant and motivational support.

I also express my sincere thanks to ***Prof. Surendra Kumar Trigun and Prof. S. Saikrishna*** Faculty of Science, Banaras Hindu University, Varanasi for their help in performing *ex vivo* studies.

I am also grateful to *all the non-teaching staff* of the Department for their timely assistance and co-operation during the period of my Ph.D. research.

I am indeed thankful to have the company of my senior *Mr. Digambar Kumar Waiker* my colleagues *Ms. Poorvi Saraf, Ms. Bhagwati Bhardwaj, Ms. Neha Singh, Mr. Debudutta Mohapatra, Mr. Gajendra T A;* my juniors *Mr. Hansal Kumar, Mr. Abhinav Singh, Ms. Samridhi, Ms. Deeksha and Mr. Kshirod* and juniors who were ever ready to provide me with all the possible help.

A special thanks to my family. Words cannot express how grateful I am to all my *family members* for all of the sacrifices that they made on my behalf and the continuous support they provided to me. Most importantly, none of this would have been possible without the love and patience of my *parents, wife, daughter, brothers, and other family members*. They have been a constant source of love, moral support, and strength all these years. I owe this achievement to them.

Last but not least, I pray for the *animals* who sacrificed themselves for the cause of my research work.

Date:

Place: IIT (BHU) Varanasi



Akash Verma

LIST OF FIGURES

Fig. No.	Figure Legends	Page No.
1.1	AD molecular mechanism and major targets involved	3
1.2	Synthesis of ACh and cholinergic neurotransmission	4
1.3	Amyloidogenic and non-amyloidogenic pathways	6
1.4	Tau hyper-phosphorylation and NFTs generation	7
2.1	Structural representation of donepezil	19
2.2	Structures of the benzylpiperidine and benzylpiperazine derivatives 1-2	20
2.3	Structures of the benzylpiperidine and benzylpiperazine derivatives 3-4	21
2.4	Structures of the benzylpiperidine and benzylpiperazine derivatives 5-8	22
2.5	Structures of the benzylpiperidine and benzylpiperazine derivatives 9-11	22
2.6	Structures of the benzylpiperidine and benzylpiperazine derivatives 12-13	23
2.7	Structures of the benzylpiperidine and benzylpiperazine derivatives 14-15	23
2.8	Structures of the benzylpiperidine and benzylpiperazine derivatives 16-18	24
2.9	Structures of the benzylpiperidine and benzylpiperazine derivatives 19-20	25
2.10	Structures of the benzylpiperidine and benzylpiperazine derivatives 21-23	26
2.11	Structures of the quinazoline derivatives 24-25	28
2.12	Structures of the quinazoline derivatives 26-27	29
2.13	Structures of the quinazoline derivatives 28-30	31
2.14	Structures of the quinazoline derivatives 31-32	32
2.15	Structures of the quinazoline derivatives 33-34	33
2.16	Structures of the quinazoline derivatives 35-36	35
2.17	Structures of the quinazoline derivatives 37-38	36
2.18	Structures of the quinazoline derivatives 39-40	37
2.19	Structures of the quinazoline scaffold containing natural derivatives	38
2.20	Drugs under clinical investigation and FDA approved in AD therapy	38
2.21	Structures of the compounds under clinical investigations	41
2.22	Structures of the compounds under clinical phase	44
2.23	FDA approved drugs for AD treatment	47
3.1	Design strategy for compound AV-1 to AV-21	52
3.2	Design strategy for compound AK-1 to AK-14	55
5.1	e-pharmacophore models representing their binding sites.	86

Fig. No.	Figure Legends	Page No.
5.2	The pharmacophore overlay of hit (ZINC000015441499) and compound AV-2 . [A] ZINC000015441499 on AChE; [B] ZINC000015441499 on BACE-1; [C] AV-2 on AChE; [D] AV-2 on BACE-1.	90
5.3	Structures of common identified hits. [A] ZINC000015441499; [B] ZINC000010322640; [C] ZINC000408991674.	91
5.4	2D binding pattern of ZINC000015441499 on [A] hAChE (4EY7) and [B] hBACE-1 (2ZJM), respectively.	94
5.5	3D binding pattern of ZINC000015441499 on [A] hAChE (4EY7) and [B] hBACE-1 (2ZJM), respectively.	94
5.6	2D binding pattern of compound AV-2 on [A] hAChE (4EY7) and [B] hBACE-1 (2ZJM), respectively.	94
5.7	3D binding pattern of compound AV-2 with [A] hAChE (4EY7) and [B] hBACE-1 (2ZJM), respectively.	95
5.8	Molecular dynamics studies of ZINC000015441499-hAChE (4EY7) docked complex. [A] Histogram showing interaction fractions with active amino acid residues; [B] Graphical representation showing percentage interactions with active site residues; [C] RMSD graph of ligand-protein (ZINC000015441499-hAChE); [D] Timeline representation showing interaction with all the amino acid residues at each time frame.	95
5.9	MD simulation analysis of AV-2 -hAChE (4EY7) docked ligand-protein complex. [A] Histogram indicating ligand interaction fractions with different amino acid residues of active sites; [B] 2D interaction diagram showing percentage interactions different amino acid residues of active sites; [C] RMSD graph of ligand-protein (AV-2 -hAChE); [D] Timeline depiction protein-ligand interactions with their respective active amino acid residues at each time frame.	96
5.10	Molecular dynamics studies of ZINC000015441499-hBACE-1 (2ZJM) docked complex. [A] Histogram showing interaction fractions with active amino acid residues; [B] Graphical representation showing percentage interactions with active site residues; [C] RMSD graph of ligand-protein (ZINC000015441499-hBACE-1); [D] Timeline representation showing interaction with all the amino acid residues at each time frame.	98

Fig. No.	Figure Legends	Page No.
5.11	MD simulation analysis of AV-2 -hBACE-1 (2ZJM) docked ligand-protein complex. [A] Histogram indicating ligand interaction fractions with different amino acid residues of active sites; [B] 2D interaction diagram showing percentage interactions different amino acid residues of active sites; [C] RMSD graph of ligand-protein (AV-2 -hBACE-1); [D] Timeline depiction protein-ligand interactions with their respective active amino acid residues at each time frame.	99
5.12	HOMO-LUMO orbital density and molecular electrostatic potential (MEP) surface of the compound AV-2 ; A & B) HOMO and HOMO-1 orbital density of compound AV-2 ; C & D) LUMO and LUMO+1 orbital density of compound AV-2 ; E) molecular electrostatic potential (MEP) surface of the compound AV-2 .	101
5.13	Graphical representation of electrophilic fukui function + ve $f(r)$ left and nucleophilic fukui function – ve $f(r)$ right of compound AV-2 .	102
5.14	ORTEP diagram of compound AV-2 obtained at 100 K.	117
5.15	Enzyme kinetics studies of compound AV-2 [A] Lineweaver-burk plot, [B] Michaelis-Menten plot, and [C] Dixon plot, [D] Enzyme reversibility study. Data are expressed as mean \pm SEM (n=3). * $p < 0.05$, ** $p < 0.01$, and *** $p < 0.001$ vs control.	122
5.16	SAR of the designed series against hAChE and hBACE-1 enzymes.	124
5.17	Thioflavin T assay of compound AV-2 , [A] self-induced A β aggregation inhibition, [B] AChE-induced A β aggregation inhibition.	127
5.18	Thioflavin T assay with NFI of compound AV-2 [A] self-induced A β aggregation inhibition, [B] hAChE-induced A β aggregation inhibition. Data are expressed as mean \pm SEM (n=3). * $p < 0.05$, ** $p < 0.01$, and *** $p < 0.001$ vs control, ns = non-significant.	127
5.19	2D and 3D AFM analysis of anti-A β aggregation potential of compound AV-2 and curcumin at different time intervals.	128
5.20	Neurotoxicity (A) and neuroprotective analysis (B) of compound AV-2 on RA/BDNF differentiated neuroblastoma cell lines. Data are expressed as mean \pm SEM (n=3). $^{***}p < 0.001$ vs control; * $p < 0.05$, ** $p < 0.01$, and *** $p < 0.001$ vs H $_2$ O $_2$ treated; ns = non-significant.	130

Fig. No.	Figure Legends	Page No.
5.21	Cell morphological study on RA/BDNF differentiated neuroblastoma cell lines, [A] Control; [B] after treatment with donepezil; [C] after treatment with compound AV-2 .	130
5.22	Histopathological examination of the different animal organs via H & E staining after acute toxicity studies; [A] Kidney tissue showing normal DCT, PCT and Glomerulus; [B] Liver tissue showing the presence of normal Kupfer cells; [C] brain tissue showing normal hippocampus and cortex after crystal violet staining; [D] Heart slice showing normal cardiac muscles; [E] change in body weight up to 14 days.	131
5.23	Effect of compound AV-2 and donepezil in cognition enhancement via scopolamine-induced Y-maze amnesia model: [A] % spontaneous alterations, [B] Total no of arm entries. Data are expressed as mean \pm SEM (n=6). $\pi\pi\pi p < 0.001$ vs control; $**p < 0.01$, and $***p < 0.001$ vs scopolamine; ns = non-significant.	133
5.24	Ex-vivo analysis of compound AV-2 [A] AChE levels in hippocampal brain and [B] Acetylcholine levels in hippocampal brain. Data are expressed as mean \pm SEM (n=6). $\pi\pi\pi p < 0.001$ vs control; $*p < 0.05$, $**p < 0.01$, and $***p < 0.001$ vs scopolamine; ns = non-significant.	134
5.25	<i>Ex-vivo</i> analysis of compound AV-2 in hippocampal brain of experimental animals: [A] MDA level, [B] SOD level, [C] GSH level, and [D] catalase level. Data are expressed as mean \pm SEM (n=6). $\pi\pi\pi p < 0.001$ vs control; $*p < 0.05$, $**p < 0.01$, and $***p < 0.001$ vs scopolamine; ns = non-significant.	135
5.26	Effect of compound AV-2 and donepezil <i>via</i> ICV $A\beta_{1-42}$ -induced Morris water maze test: (A) escape latency; (B) time spent in the platform quadrant; and (C) a number of entries to the platform zone.	137
5.27	Western blot analysis of molecular protein expressions in hippocampal brain of compound AV-2 treated rats after $A\beta$ administered (ICV). [A] Western blot representing bands; [B] Quantification of BACE-1 expression; [C] Quantification of APP expression; [D] Quantification of Tau expression. $***p < 0.001$ and $**p < 0.01$ vs $A\beta$ diseased model. Values are expressed as mean \pm SEM (n=3).	138

Fig. No.	Figure Legends	Page No.
5.28	The A β and BACE-1 expression levels estimated via IHC analysis: [A] Representing IHC images of different experimental groups; [B] Densitometric quantification of % area of A β expression; [C] Densitometric quantification of % area of BACE-1 expression. ***p < 0.001 vs Model; ns = non-significant. Values are expressed as mean \pm SEM (n=3).	139
5.29	Histopathological examination of brain hippocampal (Dentate gyrus DG): [A] control, [B] A β -treated, [C] A β +Donepezil-treated, [D] A β + AV-2 -treated, [D] % neuronal density in DG with respect to control. $\pi\pi p < 0.01$ vs control; **p < 0.01 vs A β treated.	140
5.30	Pharmacokinetic analysis of compound AV-2 representing its plasma concentration with respect to time.	142
5.31	The ORTEP diagram of compound AK-2 obtained at 100 K.	150
5.32	Molecular packing of compound AK-2 in monoclinic crystal system.	150
5.33	Crystal image of compound AK-2 during SC-XRD analysis.	150
5.34	Enzyme kinetics studies of compound AK-2 [A] Lineweaver-Burk plot, [B] Michaelis-Menten plot, and [C] Dixon plot, [D] Enzyme reversibility study. Findings are reported as the mean IC ₅₀ \pm SEM (n = 3). *p < 0.05, **p < 0.01, and ***p < 0.001 vs control. One-way ANOVA followed by Newman-Keuls Multiple Comparison test.	155
5.35	SAR of designed series against hAChE and hBACE-1 enzymes.	157
5.36	Thioflavin T assay of compound AK-2 , [A] self-induced A β aggregation inhibition, [B] AChE-induced A β aggregation inhibition.	160
5.37	Thioflavin T assay of compound AV-2 . [A] self-induced A β aggregation inhibition, [B] hAChE-induced A β aggregation inhibition. Findings are reported as the mean IC ₅₀ \pm SEM (n = 3). *p < 0.05, **p < 0.01, and ***p < 0.001 vs control, ns = non-significant. One-way ANOVA followed by Newman-Keuls Multiple Comparison test.	160
5.38	Thioflavin T experiment of compound AK-2 showed reduced fluorescence intensity.	161
5.39	[A] AFM and [B] confocal microscopic studies of A β aggregation inhibition potency of compound AK-2 and curcumin at various time intervals.	162

Fig. No.	Figure Legends	Page No.
5.40	Cell culture studies of compound AK-2 on RA/BDNF differentiated SH-SY5Y cell lines. [A] Neurotoxicity; [B] Neuroprotective analysis. Findings are reported as mean \pm SEM (n=3). *p < 0.05 and **p < 0.01 vs control; π p < 0.05 vs A β (48 hr); #p < 0.05 and ##p < 0.01 vs A β (72 hr); ns = non-significant. One-way ANOVA followed by Newman-Keuls Multiple Comparison test.	164
5.41	Histopathological examination of the different animal organs via H & E staining after acute toxicity studies; [A] Kidney tissue showing normal DCT, PCT and Glomerulus; [B] Liver tissue showing the presence of normal Kupfer cells; [C] Heart slice showing normal cardiac muscles; [D] brain tissue showing normal hippocampus and cortex after crystal violet staining; [E] change in body weight up to 14 days.	165
5.42	In-vivo efficacy of compound AK-2 via A β 1-42 induced Morris water maze test: [A] escape latency determination; Two-way ANOVA followed by Bonferroni posttest. [B] Time spent on the platform quadrant; and [C] number of entries to the platform zone. *p < 0.05 vs control and **p < 0.05 vs A β . One-way ANOVA followed by Newman-Keuls Multiple Comparison test.	167
5.43	IHC analysis for investigating the levels of A β and BACE-1: [A] Representing IHC images of different experimental groups; [B] Histogram representing A β level; [C] Histogram representing BACE-1 level. ***p < 0.001 vs Model; ns = non-significant. Findings are reported as mean \pm SEM (n=3). One-way ANOVA followed by Newman-Keuls Multiple Comparison test.	168
5.44	Histopathological examination of brain hippocampal (Dentate gyrus DG): [A] control, [B] A β -treated, [C] A β +AK-2-treated, [D] A β +Donepezil-treated [E] % neuronal density in DG with respect to control. $\pi\pi$ p < 0.01 vs control; **p < 0.01 vs A β treated.	169
5.45	[A] The histogram represents the toxicity and percent of eclosed flies of treated and untreated groups. [B] The histogram represents the percent cell viability of control and AD larval gut tissue (n= 10 gut per group) at 570 nm. *p < 0.05, **p < 0.01, and ***p < 0.001 vs control; π p < 0.05, $\pi\pi$ p < 0.01 vs AD; ns = non-significant; reported as Mean with SD. One-way ANOVA followed by Newman-Keuls Multiple Comparison test.	171

Fig. No.	Figure Legends	Page No.
5.46	(I) Stereo zoom microscopic images (A) represent the normal eye phenotype in wild type (Oregon R+), severe (B), mild (c), and rescued (D). The histogram (II) shows the percent of eye phenotypes treated with AK-2 . $\rho\rho < 0.05$, $\rho\rho\rho < 0.01$, and $\rho\rho\rho\rho < 0.001$ vs control in rescued case; $*p < 0.05$, $**p < 0.01$, and $***p < 0.001$ vs control in severe case; $\pi\pi\rho < 0.01$, and $\pi\pi\pi\rho < 0.001$ vs control in mild case. Two-way ANOVA followed by Bonferroni posttest.	172
5.47	Pharmacokinetic analysis of compound AK-2 representing its plasma concentration with respect to time.	174
5.48	Superimposition images of re-docked ligands with the co-crystallized ones. [A] on hAChE (4EY7) (RMS: 0.0189); [B] on bBACE-1 (2ZJM) (RMS:0.1752).	175
5.49	2D binding interaction of [A] donepezil and [B] compound AK-2 on hAChE active site.	177
5.50	2D binding interaction of [A] donepezil and [B] compound AK-2 on hBACE-1 active site.	178
5.51	Site mapping analysis for favorable binding site prediction on hA β (2BEG). [A] Site 1 and [B] Site 2. H-bond acceptor region (Red), H-bond donor region (Blue), Hydrophilic region (Green), Hydrophobic region (Yellow), and Metal binding region (Pink).	178
5.52	2D binding interaction of [A] curcumin and [B] compound AK-2 on hA β active site.	179
5.53	3D binding interactions of standard compounds on their respective enzymes. [A] donepezil on hAChE; [B] donepezil on hBACE-1; and [C] curcumin on hA β ₁₋₄₂ .	179
5.54	3D binding interaction of compound AK-2 with [A] hAChE (4EY7); [B] hBACE-1 (2ZJM); and [C] hA β (2BEG), respectively.	180
5.55	MD simulation study of AK-2 -hAChE (4EY7) ligand-protein docked complex. [A] RMSD graph; [B] 2D interaction diagram of compound AK-2 with the active region of hAChE; [C] Histogram revealing ligand interaction fractions with the active region of hAChE; [D] Timeline displaying protein-ligand interactions throughout 100 ns.	181
5.56	MD simulation study of AK-2 -hBACE-1 (2ZJM) ligand-protein docked complex. [A] RMSD graph; [B] 2D interaction diagram of compound AK-2 with	182

the active region of hBACE-1; [C] Histogram revealing ligand interaction fractions with the active region of hAChE; [D] Timeline displaying protein-ligand interactions throughout 100 ns.

- 5.57** MD simulation study of **AK-2**-hA β (2BEG) ligand-protein docked complex. [A] 183
RMSD graph; [B] 2D interaction diagram of compound **AK-2** with the active region of hBACE-1; [C] Histogram revealing ligand interaction fractions with the active region of hAChE; [D] Timeline displaying protein-ligand interactions throughout 100 ns.
- 5.58** HOMO-LUMO orbital density of the compound **AK-2** in gaseous environment; 186
A & C) HOMO and HOMO-1 orbital density of compound **AK-2**; B & D) LUMO and LUMO+1 orbital density of compound **AK-2**.
- 5.59** HOMO-LUMO orbital density of the compound **AK-2** in aqueous environment; 187
A & C) HOMO and HOMO-1 orbital density of compound **AK-2**; B & D) LUMO and LUMO+1 orbital density of compound **AK-2**.
- 5.60** Graphical representations of fukui functions and [A] Nucleophilic fukui function 188
- ve $f(r)$ left, [B] Electrophilic fukui function + ve $f(r)$ right.
- 5.61** Graphical representation of molecular electrostatic potential (MEP) surface of 189
the compound **AK-2**. [A] in gaseous [B] in aqueous environment.

LIST OF SCHEMES

Scheme No.	Figure Legends	Page No.
1	Synthesis of target compounds AV-1 to AV-21 .	64
2	Synthesis of designed derivatives AK-1 to AK-14 .	66

LIST OF TABLES

Table No.	Table caption	Page No.
2.1	Drugs and vaccines under clinical trials for AD therapy.	44
5.1	Table representing pharmacophoric features on hAChE and hBACE-1	88

models. [A] donepezil on hAChE; [B] F1M on hBACE-1; [C] hit ZINC000015441499 on hAChE; [D] hit ZINC000015441499 on hBACE-1; [E] AV-2 on hAChE; [F] AV-2 on hBACE-1; [G] hit SEW06622 on hAChE; and hit SEW06622 on hBACE-1.

5.2	Molecular docking score and their respective MM-GBSA, ΔG (binding free energy) of identified hits against hAChE and hBACE-1.	92
5.3	Molecular dynamics simulation analysis of identified hits and compound AV-2 .	100
5.4	QikProp analysis of compound AV-2 .	103
5.5	Crystallography and structure refinement data of compound AV-2 .	117
5.6	Structures, inhibitory profile of designed compounds against ChE (hAChE and hBuChE) and hBACE-1 enzymes and their selectivity.	119
5.7	The PAMPA-BBB permeability and PI displacement assay for screened compounds.	126
5.8	Liver and kidney function test of experimental animals under acute toxicity studies.	131
5.9	The findings of Pharmacokinetic analysis after oral administration of compound AV-2 (20 mg/kg).	141
5.10	Crystal data and structure refinement for AK-2	150
5.11	Inhibitory profile of the synthesized compounds (AK-1 to AK-14) against hChE and hBACE-1 enzymes.	153
5.12	The PAMPA-BBB permeability and PI displacement assay for screened derivatives AK-1 to AK-3 .	158
5.13	Liver and kidney function test of experimental animals under acute toxicity studies.	165
5.14	The pharmacokinetic profile of orally administered compound AK-2 (20 mg/kg).	174
5.15	Docking scores of the compounds and standard with [A] hAChE and [B] hBACE-1 enzymes.	180
5.16	MM-GBSA analysis of compound AK-2 with hAChE, hBACE-1, and hA β enzymes.	184
5.17	ADME drug-likeness analysis of compound AK-2 .	185

ABBREVIATIONS AND SYMBOLS

ACh	Acetylcholine
AChE	Acetylcholinesterase
AD	Alzheimer's disease
AFM	Atomic force microscopy
AMP	Adenosine monophosphate
AMPK	AMP-activated protein kinase
AP	Anterior – Posterior
ApoE	Apolipoprotein E
A β	Amyloid beta
APP	Amyloid precursor protein
ATCI	Acetylthiocholine iodide
ATR	Attenuated total reflectance
BACE-1	Beta amyloid cleaving enzyme 1
BBB	Blood-brain barrier
BChE	Butyrylcholinesterase
BSA	Bovine serum albumin
BTCI	Butyrylthiocholine iodide
CADD	Computer-aided drug design
CAS	Catalytic anionic site
CAT	Choline acetyltransferase
CDCl ₃	Deuteriochloroform
CDK-5	Cyclin dependent kinase-5
ChE	Cholinesterase
CNS	Central nervous system
CoA	Coenzyme A
COX	Cyclooxygenase
CREB	Cyclic-AMP-response element-binding protein
CST	Conjugated secondary antibody
CYP	Cytochrome P
DMSO	Dimethyl sulfoxide
DPP	Docking-post processing
DTNB	5,5-Dithio-bis-(2-nitrobenzoic acid)
DV	Dorsal - Ventral
EDGs	Electron donating groups
EDTA	Ethylenediaminetetraacetic acid
ELT	Escape latency time

ERK	Extracellular signal-regulated protein kinases
EtOH	Ethanol
EWGs	Electron withdrawing groups
FDA	Food and drug administration
FRET	Fluorescence resonance energy transfer
FT-IR	Fourier-transform infrared spectroscopy
GSK-3 β	Glycogen synthase kinase-3 β
hAChE	Human AChE
hBChE	Human BChE
HPLC	High performance liquid chromatography
HTVS	High throughput virtual screening
i.p.	Intraperitoneal
ICV	Intracerebroventricular
LBDD	Ligand-based drug design
MAO-B	Monoamine oxidase-B
MAPK	Mitogen activated protein kinase
MARK	Microtubule affinity-regulating kinase
MDA	Malondialdehyde
ML	Medial – Lateral
MM-GBSA	Molecular mechanics generalized Born surface area
mp	Melting point
MTT	3-(4,5-Dimethylthiazol-2-yl)-2,5-diphenyl-tetrazolium bromide
Na-CMC	Sodium carboxymethyl cellulose
NADPH	Reduce form of nicotinamide adenine dinucleotide phosphate
NFI	Normalized fluorescence intensity
NFTs	Neurofibrillary tangles
NMDAR	<i>N</i> -Methyl-D-aspartate receptor
NMR	Nuclear magnetic resonance spectroscopy
NOS	Nitric oxide synthase
NO _x	NADPH oxidase
NPT	Normality, pressure and temperature
OECD	Organisation for economic co-operation and development
OPLS	Optimized potential for liquid simulations
p.o.	Per oral
PAMPA	Parallel artificial membrane permeation assay
PAS	Peripheral anionic site
PBL	Porcine brain lipid

PBS	Phosphate buffered saline
PBST	Phosphate buffered saline with Tween 20
PDB	Protein data bank
PDE	Phosphodiesterase
PHFs	Paired helical fibrils
PI	Propidium iodide
PKA	Protein kinase-A
PPs	Protein phosphatases
PTPA	Protein tyrosine phosphatase-A
QSAR	Quantitative structure-activity relationship
RIPA	Radioimmunoprecipitation assay
RMSD	Root mean square deviation
RNS	Reactive nitrogen species
ROS	Reactive oxygen species
SBDD	Structure-based drug design
SFKs	Src family non-receptor tyrosine kinases
SOD	Superoxide dismutase
SP	Standard precision
TBARS	Thiobarbituric acid reactive substances
TBST	Tris-buffered saline with Tween 20
TLC	Thin layer chromatography
TPKI	Tau protein kinase-I
TRITC	Tetramethylrhodamine isothiocyanate
UV	Ultraviolet spectroscopy
VSGB	Variable surface generalized Born
WHO	World Health Organization
XO	Xanthine oxidase
XP	Extra precision
XRD	X-ray diffraction

SYMBOLS & UNITS

× g	Relative centrifugal force
°C	Degree Celsius
μL	Microliter
μm	Micrometer
μM	Micromolar
Å	Angstrom
α	Alpha

β	Beta
γ	Gamma
ν	Wavenumber
cm	Centimeter
d	Doublet
dd	Doublet of doublets
ddd	Doublet of doublets of doublets
equiv	Equivalent
g	Gram
h	Hour
Hz	Hertz
<i>J</i> -value	Spin-spin coupling constant
K	Kelvin
kg	Kilogram
KHz	Kilohertz
m	Multiplet
mg	Milligram
min	Minute
mL	Milliliter
mM	Millimolar
ng	Nanogram
nm	Nanometer
q	Quartet
RH	Relative humidity
rpm	Rotations per minute
s	Seconds/Singlet
t	Triplet
td	Triplet of doublets
U/mL	Units per milliliter
v/v	Volume by volume
w/v	Weight by volume

PREFACE

Alzheimer's disease (AD) has been identified to be a major health issue caused on by the degeneration of neurons and synapses, especially in the hippocampus and neocortex. AD results in anatomical and functional brain damage which causes severe behavioral changes and cognitive dysfunction. According to a 2018 World Health Organization (WHO) assessment, there are 50 million cases of AD globally, and by 2050, this number is expected to triple.

Lower acetylcholine (ACh) levels in the synaptic cleft, amyloid beta ($A\beta$) aggregation and deposition, N-methyl-D-aspartate receptor (NMDAR) activation, oxidative stress in response to neuroinflammation, tau hyperphosphorylation that leads to the formation of neurofibrillary tangles (NFTs), genetic mutation in apolipoprotein E4 ($APO\epsilon 4$), etc. are some of the underlying pathophysiologies linked to the progression of cognitive deficits in the AD condition.

The current treatment strategy for AD involves the use of some FDA-approved drugs which only provide symptomatic relief to the patient. Certain FDA-approved medications such as AChE inhibitors (donepezil, rivastigmine, and galantamine) and NMDA receptor antagonists (memantine) are being used for the treatment of AD. Recently, Aducanumab and Lecanemab (monoclonal antibodies) have been approved by FDA in an accelerated approval pathway as a disease-modifying therapy for AD, though their use is still controversial in AD progression.

This research work in this thesis was divided into two parts; the first part of the thesis describes the design, synthesis of a novel series-I (**AV-1 to AV-21**) containing quinazoline derivatives based on the structure based drug design approach and biologically evaluated them against hAChE, hBChE, hBACE-1, and $A\beta$ aggregation inhibitory potentials. The type

of enzyme inhibition was also estimated using enzyme kinetic study of the most potent compound against hAChE enzyme. The PAMPA-BBB and propidium iodide displacement assay were also carried out to check that the most promising compound was able to permeate the BBB barrier with significant PAS binding, respectively. The neurotoxic liabilities and neuroprotective properties of the compounds were also tested against RA/BDNF differentiated SH-SY5Y neuroblastoma cell lines. A detailed *in-vivo* study of the most active compound of the series was also performed in scopolamine and A β -induced behavioral rat models of AD following *ex-vivo* biochemical estimation of various oxidative biomarkers, and histopathological examination of brain tissue slices to observe any neuronal tissue damage. The molecular expression levels of A β , BACE-1, and APP were also estimated using western blotting and IHC analysis. The *in-silico* molecular docking, molecular dynamic simulation studies, and DFT studies were also performed to confirm the ligand-protein complex's stability and overall electronic properties of the active compound. The *in-vivo* BBB permeability and pharmacokinetic analysis of the active compound were also performed.

The second part of the thesis demonstrates the lead optimization based design of quinazoline derivatives (**AK-1** to **AK-14**) using bioisosteric and molecular hybridization approach. The designed series II were synthesized and biologically evaluated for their *in-vitro* inhibitory potential against hAChE, hBChE, hBACE-1, and A β aggregation. The neurotoxic liabilities and neuroprotective properties of the compound were also tested against RA/BDNF differentiated SH-SY5Y neuroblastoma cell lines. The A β -induced mouse model for AD was studied to evaluate the learning and memory behavior improvements after treatment with the most active compound of the series. *Ex-vivo* studies of hippocampal brain homogenates were performed to investigate the oxidative stress biomarker. The molecular expression levels of

A β and BACE-1 were also estimated using IHC analysis. The histopathological examination was performed to observe neuronal appearance in the hippocampal region of the brain. The *Drosophila* eye phenotypic AD model was also performed to check that the active compound possess anti-A β aggregation potential. The *in-vivo* BBB permeability and pharmacokinetic analysis of the active compound were also performed.

The work has been presented in this dissertation under the following sections:

Chapter 1: The pathophysiology, development, and course of AD are briefly discussed in this chapter. It also covers the current treatment strategies for AD, more recent design approaches including computational and molecular hybridization approaches that focuses mostly on to slow the progression of the AD.

Chapter 2: This chapter describes a detailed literature survey on N-benzylpiperidines, benzylpiperzines, quinazoline derivatives, drugs under clinical investigations, and FDA approved drugs against AD.

Chapter 3: This chapter summarizes the research objectives of the overall study, the rationale for performing different *in vitro* and *in vivo* investigations, and a detailed plan of work that is exemplified in this thesis.

Chapter 4: This chapter describes the experimental procedure used in the synthesis, characterization, protocols for computational studies, and *in vitro* and *in vivo* pharmacological evaluations.

Chapter 5: This chapter covers the overall findings as results and discussion part of the research work.

Chapter 6: Describes the summary and conclusion of the presented work.

Chapter 7: This section includes the references as a source of information to carry out the research work.

Chapter 8: An appendix consisting of the NMR (^1H and ^{13}C) and Mass spectra along with HPLC chromatograms of the representative compounds followed by a list of published papers and presentations at international conferences.